

An Immunomodulator-Boosted Lactococcus Lactis Platform For Enhanced In Situ Tumor Vaccine

Mengna Sun, Tianyu Shi, Subiyinuer Tuerhong, Mengru Li, Qiaoli Wang, Changchang Lu, Lu Zou, Qinghua Zheng, Yingxin Wang, Juan Du, Rutian Li,* Baorui Liu,* and Fanyan Meng*

In situ vaccination is an attractive type of cancer immunotherapy, and methods of persistently dispersing immune agonists throughout the entire tumor are crucial for maximizing their therapeutic efficacy. Based on the probiotics usually used for dietary supplements, an immunomodulator-boosted *Lactococcus lactis* (IBL) strategy is developed to enhance the effectiveness of in situ vaccination with the immunomodulators. The intratumoral delivery of OX40 agonist and resiquimod-modified *Lactococcus lactis* (OR@Lac) facilitates local retention and persistent dispersion of immunomodulators, and dramatically modulates the key components of anti-tumor immune response. This novel vaccine activated dendritic cells and cytotoxic T lymphocytes in the tumor and tumor-draining lymph nodes, and ultimately significantly inhibited tumor growth and prolonged the survival rate of tumor-bearing mice. The combination of OR@Lac and ibrutinib, a myeloid-derived suppressor cell inhibitor, significantly alleviated or even completely inhibited tumor growth in tumor-bearing mice. In conclusion, IBL is a promising in situ tumor vaccine approach for clinical application and provides an inspiration for the delivery of other drugs.

treatment in the past decade. On the one hand, ISV makes the tumor itself a vaccine factory, continuously activating the anti-tumor immune response and converting the immunosuppressive microenvironment into an immunostimulatory one.^[1] On the other hand, it avoids the off-target toxic side effects associated with systemic immune stimulation.^[2,3] To enhance tumor immunogenicity and make it a “self-vaccine”, multiple strategies have been incorporated into the configuration of in situ vaccine. Among these strategies, the combination of immunomodulatory proteins and small molecule immunoagonists has received extensive attention.^[1,4] This combination strategy of direct intratumoral co-administration can eradicate tumors by triggering a specific T-cell immune response.^[1] As a member of the co-stimulatory receptors on T cells, OX40 has the function of T cell activation and is one of the most widely studied immunoregulatory protein agonists.^[5] The OX40-OX40L interactions have been reported to be conducive to the primary T cell stimulation and expansion, facilitating the establishment of long-term effector T cells and memory T cells.^[6] Single administration of the OX40 agonist (α OX40) did not meet the expectations of clinical trials.^[7,8] Given the limitations of this

1. Introduction

In situ vaccination (ISV) composed of antigens and/or adjuvants have been a promising immunotherapeutic approach for cancer

primary T cell stimulation and expansion, facilitating the establishment of long-term effector T cells and memory T cells.^[6] Single administration of the OX40 agonist (α OX40) did not meet the expectations of clinical trials.^[7,8] Given the limitations of this

M. Sun, T. Shi, S. Tuerhong, M. Li, Q. Wang, L. Zou, Y. Wang, J. Du, F. Meng
Department of Comprehensive Cancer Centre
Nanjing Drum Tower Hospital
Clinical College of Traditional Chinese and Western Medicine
Nanjing University of Chinese Medicine
Nanjing 210008, China
E-mail: fanyanmeng@nju.edu.cn

Q. Zheng, Y. Wang, F. Meng
Department of Laboratory Medicine
Nanjing Drum Tower Hospital
Affiliated Hospital of Medical School
Nanjing University
Nanjing 210008, China

M. Sun, T. Shi, S. Tuerhong, M. Li, Q. Wang, C. Lu, L. Zou, Q. Zheng, Y. Wang, J. Du, R. Li, B. Liu, F. Meng
Department of Comprehensive Cancer Centre
Nanjing Drum Tower Hospital
Affiliated Hospital of Medical School
Nanjing University
Nanjing 210008, China
E-mail: rutianli@nju.edu.cn; baorui.liu@nju.edu.cn

Q. Zheng
Department of Comprehensive Cancer Centre, Nanjing Drum Tower Hospital, Joint Institute of Nanjing Drum Tower Hospital for Life and Health
College of Life Science
Nanjing Normal University
Nanjing 210008, China

The ORCID identification number(s) for the author(s) of this article can be found under <https://doi.org/10.1002/adhm.202401635>

DOI: 10.1002/adhm.202401635

monotherapy, α OX40 is currently mainly explored in combination with small molecule immune drugs.^[4,9,10] However, it is difficult to maintain their effective accumulation and persistent retention of small molecule anti-tumor drugs at the tumor site, because of the inhibition of their efficacy through tumor vascular and/or lymphatic metabolism.^[11]

Transporting drugs into the tumor microenvironment (TME) and maintaining their efficacy has been a fanatical question for decades.^[12] Currently, a wide range of complex vectors, such as liposomes, inorganic nanoparticles, polymer nanogel, and injectable hydrogels, have been developed to deliver immune adjuvants and antigenic proteins/peptides, and then concentrate drugs into tumor tissues through enhanced permeability and retention effect.^[13,14] Despite achieving some incremental results, the overall effectiveness remains limited due to the influence of multiple biological barriers.^[15] Probiotics have the special advantages as tumor vaccines, as they can serve as both biological vectors for drug transportation and as good immune adjuvants to active innate and adaptive immunity.^[16] On one hand, due to the immunosuppressive and hypoxic tumor microenvironment alongside bacterial motility, therapeutic probiotic formulations exhibit exceptional tumor-targeting capabilities, rendering them as capable of serving as delivery vehicles for cancer in situ vaccination.^[12] On the other hand, some probiotics have been reported to be rich in a large number of pathogen-associated molecular patterns, which effectively modulate the immune system.^[16] Considering safety and practicality, food-grade *Lactococcus lactis* (*L. lactis*) has enormous potential for tumor immunotherapy. As a facultative anaerobic bacterium, it exhibits a propensity to target and localize within the TME.^[17]

Here, we present an innovative in situ vaccine strategy that α OX40 and resiquimod (R848) were modified to the surface of *L. lactis*, resulting in the generation of dual immune adjuvant modified *L. lactis* (OR@Lac). R848, a small-molecule immunomodulatory, belongs to the Toll-like receptor 7/8 (TLR7/8) agonist family. Upon binding of R848 to TLR7/8 receptor, a diverse array of cytokines such as IL-6 and TNF- α are released, initiating a series of signaling pathways that facilitate the activation of antigen-presenting cells.^[18,19] The combination of the two drugs is expected to fulfill the requirements of innate immunity and adaptive immunity in the anti-tumor immunity. In this design, intratumoral injection (i.t.) of OR@Lac can facilitate efficient antigen cross-presentation by dendritic cells (DCs) within the TME and tumor draining lymph nodes (TDLNs). *L. lactis* served as a living carrier for drug delivery, transporting immune drugs to various parts of tumor tissue to play a combined therapeutic role. Our research demonstrated that the IBL strategy induced significant tumor regression and triggered robust systemic immune response by augmenting the population of mature DCs and restoring cytotoxic T lymphocytes (CTLs) (Figure 1). In the subsequent analysis of the TME, we found substantial accumulation of myeloid-derived suppressor cells (MDSCs) in the tumors, leading to subsequent tumor progression and recurrence. Therefore, we further administered ibrutinib, an MDSC inhibitor, to regulate the production and function of MDSC.^[20] The synergy between OR@Lac and ibrutinib significantly enhanced the anti-tumor effect, indicating that our approach provides an attractive strategy for in situ tumor vaccines.

2. Results

2.1. Preparation and Characterization of OR@Lac

The inherent characteristics of *L. lactis* endow them with the mobility and adaptability to target location and perform certain functions within the TME, which demonstrated strong capabilities for TME-targeted drug delivery. The preparation of OR@Lac is schematically illustrated in Figure 2a. The cell wall of *L. lactis* is rich in N-acetylmuramic acid and N-acetylglucosamine.^[21] Through one-step amide condensation, aminated R848 and α OX40 were attached to the carboxyl group of N-acetylmuramic acid on the surface of *L. lactis*, which are extensively found in the cell wall of bacteria and exhibits more reactive than other carboxyl groups.^[22–24] Briefly, OR@Lac was prepared by separately co-incubating *L. lactis* with R848 and α OX40 in PBS at room temperature for 2 h with the help of EDC and NHS. Subsequently, the resulting OR@Lac was purified by centrifugation. Then we tested the loading efficiency of R848 and α OX40, and determined by HPLC that the loading efficiency of R848 was 49.42%, while the loading efficiency of α OX40 was 22.93% (Table S1, Supporting Information.). Typical TEM and SEM images were displayed R848 coupled with α OX40 onto the bacterial surface did not change its original shape (Figure 2b; Figure S1, Supporting Information). DLS analysis showed that the mean size of OR@Lac after conjugation increased from 1.15 to 1.41 μ m compared to Lac, with no significant change in zeta potential (Figure 2c,d). Notably, unaffected bacterial viability is essential for OR@Lac to penetrate thoroughly in tumor tissue.^[25] We found that the surface modification process of R848 and α OX40 had limited side effects on bacterial viability, and thus the proliferation of OR@Lac was similar to that of unmodified bacteria (Figure 2e). Then, we detected whether α OX40 could be integrated onto the *L. lactis* surface, cy5-conjugated α OX40 was employed and measured by flow cytometry and immunofluorescence microscope. As shown in Figure 2f, flow cytometry analysis showed the successful decoration with α OX40, the average fluorescence intensity of α OX40@Lac was significantly higher than that of Lac group (Figure 2g). Immunofluorescence images also further confirmed that bacteria are effectively modified with red fluorescence under the experimental condition (Figure 2h).

2.2. OR@Lac Effectively Induced the Activation of BMDCs and T Cells In Vitro

The induction of antigen-specific immune response requires effective interactions between specialized antigen-presenting cells (APCs) and antigen-specific T cells.^[26] As the key APCs, the recognition and internalization of antigens by DCs are essential steps in processing and presenting tumor-specific antigens. After antigen capture, immature DCs migrate into the TDLNs for maturation, followed by the upregulation of costimulatory molecule expression and cytokine secretion.^[27] To determine the activation ability of DCs, different processing groups were directly co-cultured with bone marrow-derived dendritic cells (BMDCs) for 24 h. The immunostimulatory activity was evaluated via flow cytometry, as shown in Figure 3a,b, all groups containing R848 significantly induced the maturation of BMDCs (CD80⁺CD86⁺),

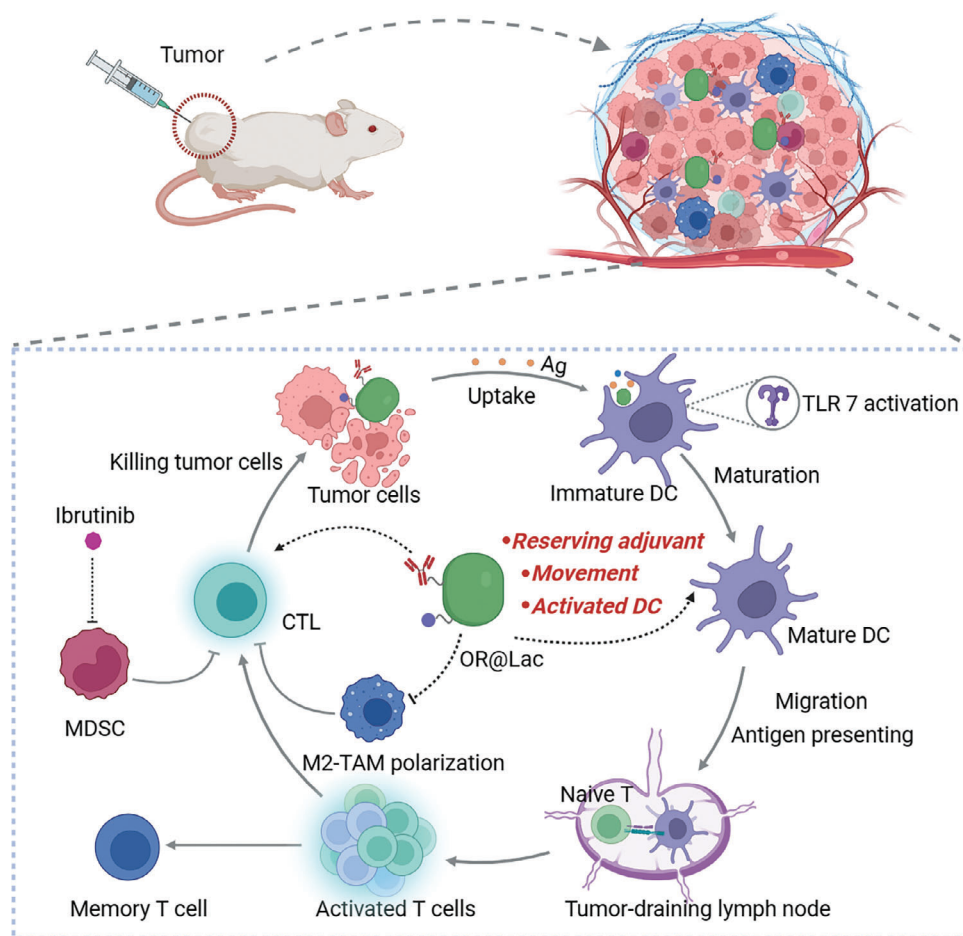


Figure 1. Schematic diagram of intratumorally injecting OR@Lac combined with ibrutinib therapy to enhance tumor immunotherapy and the mechanism of anti-tumor immune response.

which is consistent with previous reports.^[18,28] As expected, treatment with OR@Lac greatly upregulated the expression of costimulatory molecules on BMDCs compared to both Lac and OR groups, indicating enhanced DC activation. Notably, the Lac group alone significantly increased the percentages of mature BMDCs compared to the NS group due to the natural immunogenicity of the *L. lactis*. In addition, the OR@Lac group had significantly higher secretion of $\text{TNF-}\alpha$, IL-6, and $\text{INF-}\gamma$, which played key roles in initiating and stimulating innate immune response (Figure 3c–e). To further examine the internalization of *L. lactis* by BMDCs, DIO stained *L. lactis* and DiI stained BMDCs were co-incubated at a ratio of 10:1 for 2 h. As shown in Figure 3f, most BMDCs internalized these *L. lactis*. These results demonstrated that OR@Lac could be effectively uptake by DCs, leading to a stronger immune responses and enhanced vaccination.

Once immature DCs reach maturation, they stimulate immune responses that activate T cells through surface antigen presentation. Next, we assessed the levels of T cell activation. Following co-incubation of BMDCs with OR@Lac, BMDCs were mixed with T cells for 72 h to evaluate the expression of CD69, an early activation marker. The expression of $\text{CD4}^+\text{CD69}^+$ and

$\text{CD8}^+\text{CD69}^+$ induced by OR@Lac treated BMDCs increased by about twice compared to the NS group (Figure 3g,h).

2.3. OR@Lac Induced Persistent Intratumoral Distribution and Drug Retention

ISV is an effective strategy to increase the accumulation and retention of therapeutic drugs at the tumor site.^[2] To confirm the motility and biodistribution of *L. lactis* in vivo, we performed a signal intratumoral injection of DIR-labeled *L. lactis* and then visualized the distribution using an in vivo imaging system (IVIS). All injected *L. lactis* were predominantly trapped in the core of the tumor, peaking at 72 h and then waning until 360 h post-treatment consistent with previous research.^[16] Central organs, tumors, and TDLNs were excised at different time points and measured in vitro (Figure 4b,c). It is noteworthy that fluorescent signals were detectable in TDLNs within 24 h, presenting an excellent opportunity for immune activation in TDLNs.

Conventional small-molecule drugs can be rapidly eliminated after local injection and are difficult to disperse to distant tumor tissues.^[29] Although intratumoral or peritumoral injections of liposomes or gel-like drug delivery systems can enhance tu-

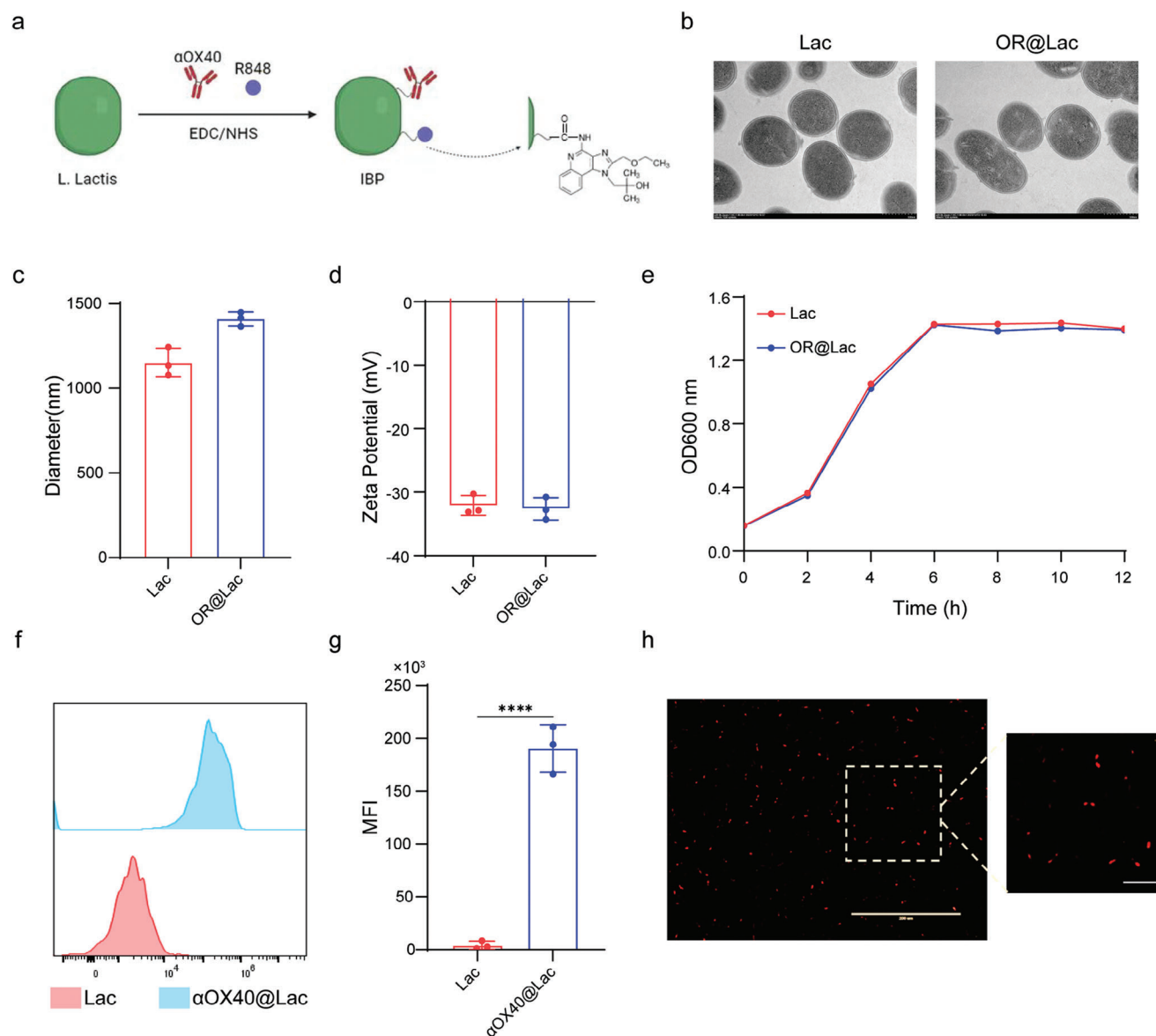


Figure 2. Preparation and characterization of decorated *L. lactis*. **a**) Schematic diagram of attaching R848 and α OX40 onto the surface of bacteria via amide condensation under EDC/NHS catalytic conditions. **b**) Representative TEM images of Lac and OR@Lac, respectively. Scale bar: 500 nm. **c,d**) The diameters and zeta potentials of free Lac and OR@Lac measured by DLS, error bars based on SD ($n = 3$). **e**) Growth curves of Lac and OR@Lac cultured in GM17 medium at 30 °C ($n = 3$). **f**) The representative flow cytometry histograms of Lac and α OX40@Lac (cy5.5 labeled α OX40). **g**) The mean fluorescence intensity of Lac and α OX40@Lac ($n = 3$). **h**) Typical immunofluorescence images of α OX40@Lac (cy5.5 labeled α OX40). Scale bar: 200 μ m. Data were mean \pm SD. Student's *t*-test was used for statistical analysis.

mor retention, therapeutic drugs only concentrate at the point of injection or tumor edge and prevent them from penetrating deeply into the tumor due to the influence of dense extracellular matrix and intratumoral pressure.^[30,31] Considering the preference of *L. lactis* colonization at tumor sites, we used IgG to study the distribution of IgG in free and IgG@Lac injected into CT26 tumor-bearing mice. As expected and supported by the IVIS image, tumor colonization of IgG@Lac greatly prolonged tumor retention time of conjugated IgG, whereas the IgG in free form were cleared faster (Figure 4d,f). Furthermore, the quantitative analysis demonstrated that at 48 h post-injection, the signal in-

tensity of IgG@Lac was significantly higher than that of the free IgG group and ≈ 4.7 times higher at 72 h (Figure 4e,g), reflecting a prolonged retention mediated by *L. lactis*. In addition, we further examined the injection IgG@Lac intratumoral distribution of post IgG. 72 h after injection of FITC labeled free IgG and IgG@Lac. As shown in Figure 4h, the distribution of IgG in the deep tumor area was observed in the IgG@Lac group, while the immunofluorescence in the free IgG group was almost negligible. In conclusion, the preferential colonization and motility of *L. lactis* at the tumor site endowed OR@Lac with the capability to uniformly and continuously release immunomodulators.

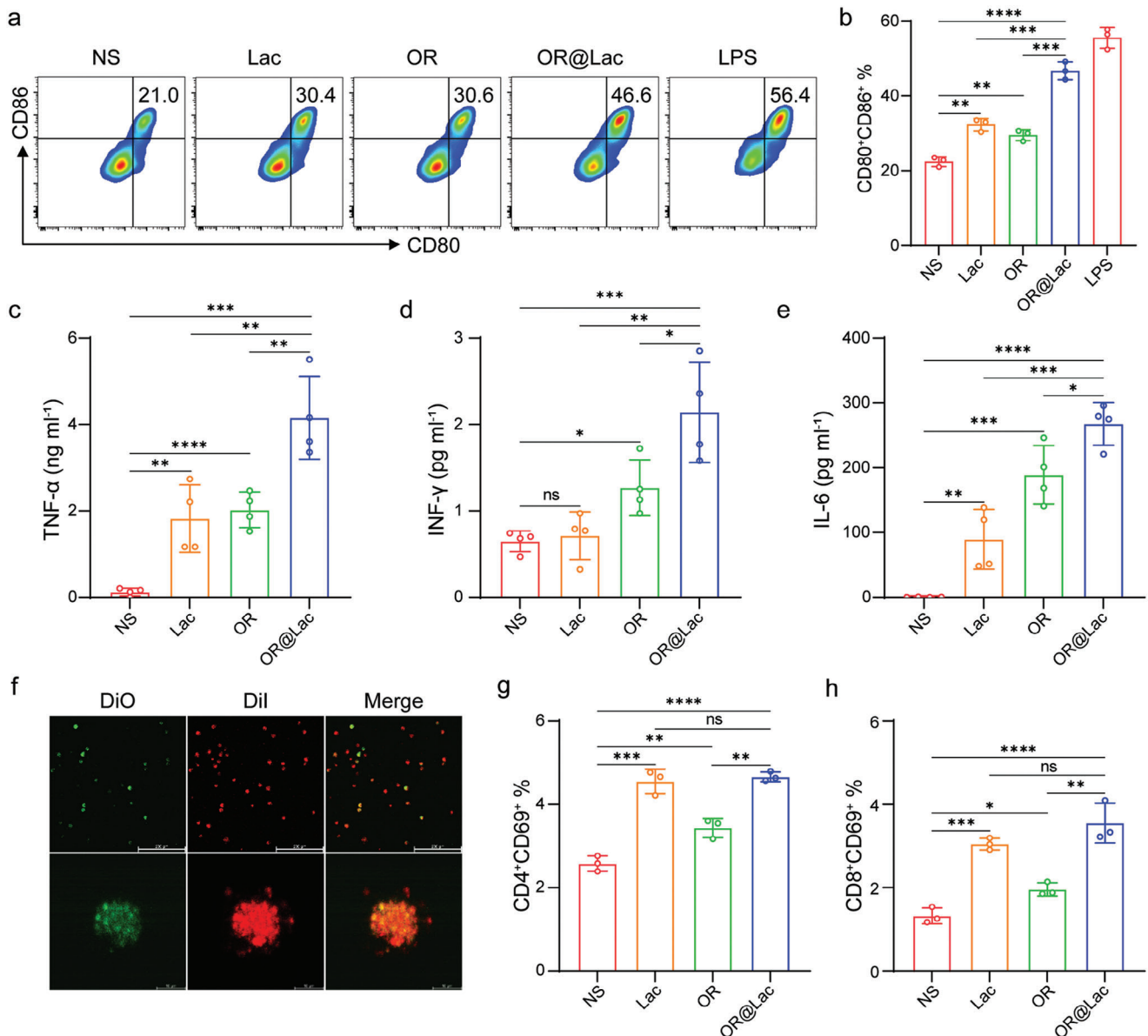


Figure 3. In vitro activation of BMDCs and T cells. a,b) Representative flow cytometry images and the percentage of mature DCs (CD80⁺CD86⁺) after co-incubation with saline, Lac, OR, OR@Lac, and LPS for 24 h (n = 3). c–e) Percentage of pro-inflammatory cytokine concentrations in BMDC supernatants (n = 4). f) Colocalization analysis of *L. lactis* (DiO; green) in BMDCs (DiI; red) by confocal microscopy after co-incubation 2 h. White scale bars: 50 μm. g,h) The percentage of CD69 expression on CD4⁺ and CD8⁺ T-cell subsets in the T cells (n = 3). For (b–e), (g,h), data were mean ± SD. Student's *t*-test was used for statistical analysis.

2.4. In Vivo Anti-Tumor Efficacy of OR@Lac in Subcutaneous and Orthotopic Tumor Models

First, we utilized a subcutaneous CT26 tumor model in BALB/c mice to evaluate the therapeutic efficacy of R848 and αOX40 combined in vivo. As shown in Figure 5a and 2×10^6 CT26 tumor cells were inoculated near the left groin of BALB/c mice. When the tumor volume reached 80–100 mm³, they were randomly divided into 4 groups for treatments. After the first injection, the treatment was repeated twice every two days, and then we monitored the tumor growth with calipers. As shown in Figure 5b, the tumors of NS-treated mice showed progressive growth, tu-

mor growth trends treated by αOX40 or R848 alone were slightly slowed, while the combined use of αOX40 and R848 treatment group significantly delayed tumor growth. Consistently, the survival of mice in the combined treatment group was obviously longer than any other groups, but did not completely inhibit tumor growth (Figure 5c).

In order to evaluate the value of immunomodulators-modified *L. lactis* in treating solid tumors, we then further explored potential effective treatments of decorated *L. lactis* in CT26 tumor models. On the 7th day of tumor inoculation, 5×10^8 CFU OR@Lac were administered through intratumoral injection as the initial immunization, NS, *L. lactis* and OR were separately injected

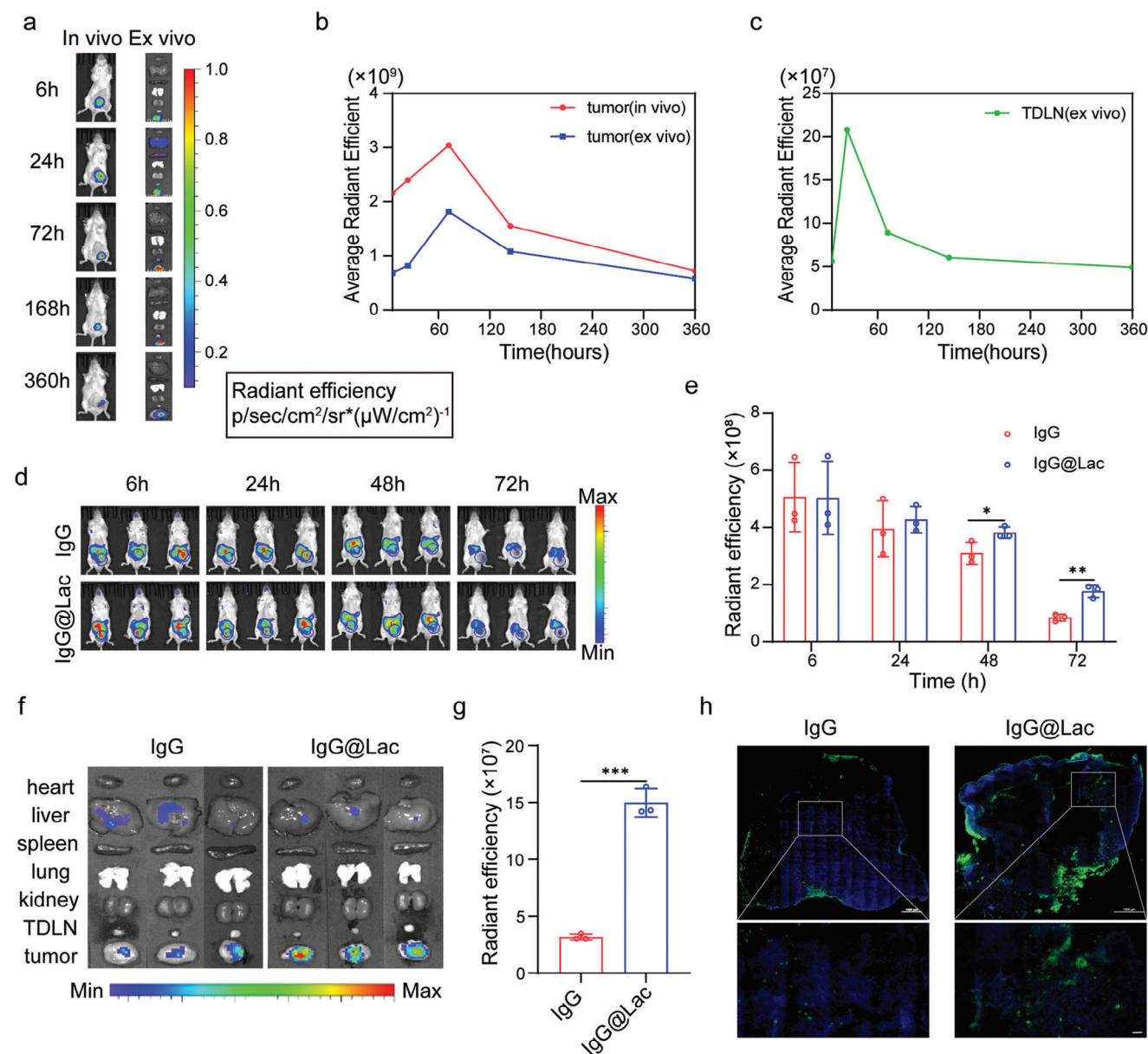


Figure 4. Temporal colonization, intratumoral retention, and distribution. a) Left, representative in vivo fluorescence imaging of tumor-bearing mice after intratumoral injection of 5×10^8 CFU *L. lactis* ($n = 3$). Right, representative ex vivo images were collected at different time points after injection. Average radiant efficiency of *L. lactis* signal in tumor tissue (b) and TDLN (c) detected in vivo or ex vivo at different time points. d) IVIS images at 6, 24, 48 and 72 h after intratumoral injection with 20 μg free cy5.5-IgG or equivalent conjugated cy5.5-IgG (5×10^8 CFU IgG@Lac) per mouse, respectively ($n = 3$). e) Average radiant efficiency of IgG and IgG@Lac at tumor site after injection ($n = 3$). f) IVIS images of major organs and tumor tissues 72 h after injection ($n = 3$). g) Average radiant efficiency of sectioned tumor tissues ($n = 3$). h) Representative fluorescence images of tumor tissue sections ($n = 3$). Green indicates FITC-IgG and FITC-IgG@Lac. Scale bar: above: 1000 μm , below: 50 μm . For e and g, data were mean \pm SD. Student's *t*-test was used for statistical analysis.

as controls. Compared with the other groups, OR@Lac group showed an effective growth inhibition on tumors, and the treatment of OR@Lac exhibited the smallest tumor volume and tumor weight, all of which were attributed to the antitumor effect of the immunomodulators-modified *L. lactis* strategy (Figure 5d–g). The reduced rate of tumor progression in the OR@Lac group significantly extended survival in the treated mice compared to all controls, 40% (2/5) of mice achieved complete tumor regres-

sion (CR) (Figure 5h). In addition, all cured mice were attacked by CT26 after 60 days, and tumor growth was completely inhibited (Figure S2, Supporting Information). The fluctuation of body weight in each group was negligible in CT26 tumor models (Figure 5i). In addition, compared to the control group, there was no significant morphological damage was observed in H&E stained histological sections of CT26 tumor model (Figure S3, Supporting Information).

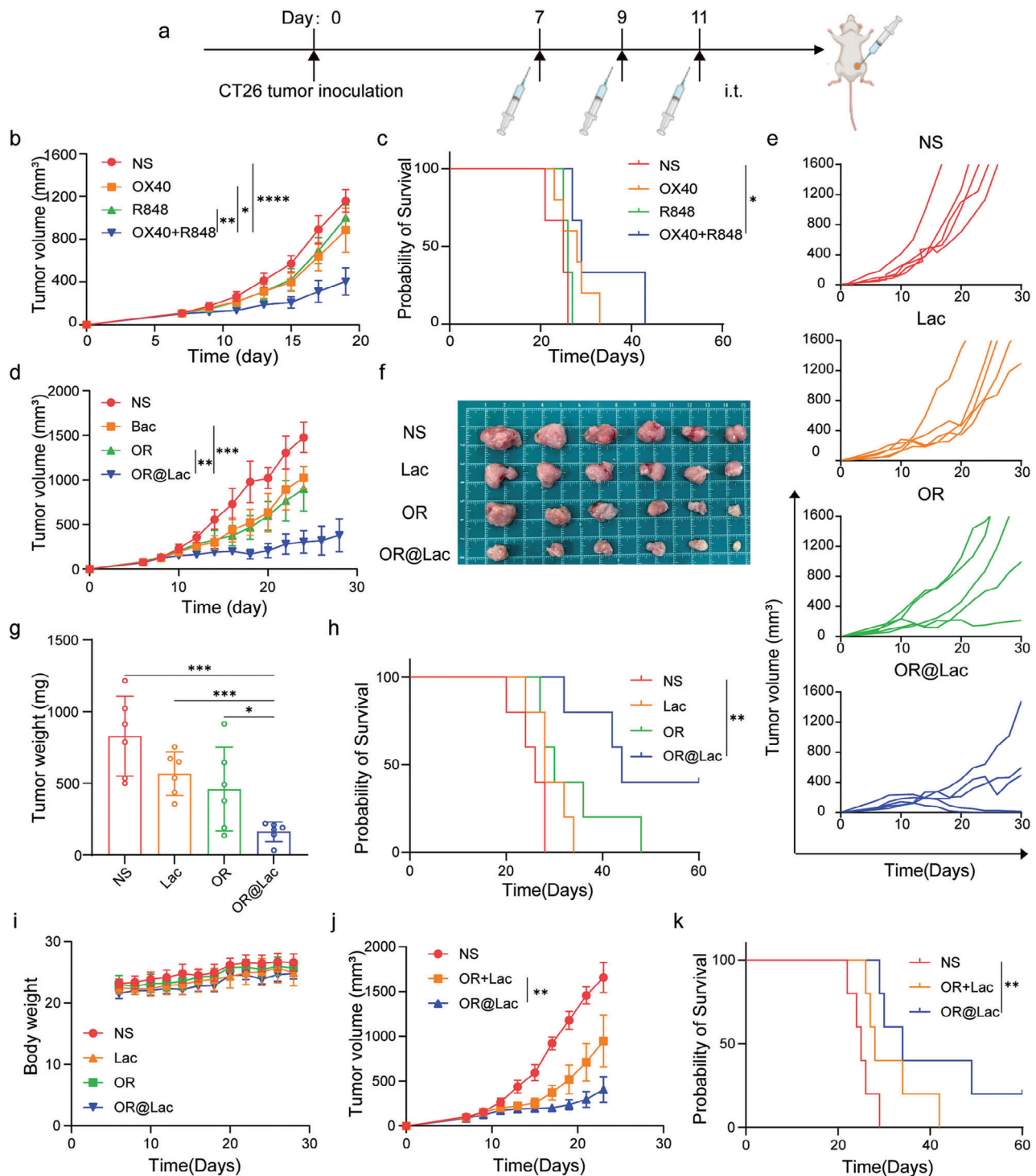


Figure 5. In vivo anti-tumor efficacy in CT26 tumor models. a) Schematic diagram of the treatment in the tumor suppression experiment. Average tumor-growth curves (b), Survival curves (c) of CT26 mice treated with NS, α OX40 (2 μ g), R848 (5 μ g) and OR (2 μ g α OX40 and 5 μ g R848) ($n = 5$). Average tumor growth curves (d), the individualized tumor growth curves (e) of CT26 mice with different treatments as indicated; (i) NS (ii) Lac (5×10^8 CFU) (iii) OR (2 μ g α OX40 and 5 μ g R848) and (iv) OR@Lac (5×10^8 CFU L. lactis contained 2 μ g α OX40 and 5 μ g R848) ($n = 5$). Photographs (f) and tumor weight (g) harvested from BALB/c mice bearing CT26 colon tumor on the 18th day after tumor inoculation ($n = 6$). h) Survival curves of mice after different treatments ($n = 5$). i) Average weight of different groups for 30 days of BALB/c mice ($n = 5$). Tumor growth curves (j), Survival data (k) of BALB/c mice bearing CT26 colon tumor treated with: (i) NS, (ii) OR+Lac, (iii) OR@Lac ($n = 5$). For the experiments in (b, d, and j), the data was the mean \pm SEM. p -values were calculated by two-way ANOVA with Tukey's multiple comparisons test and correction. Survival differences were determined using Kaplan–Meier methods, and P -values were calculated using logarithmic rank (Mantel–Cox) tests. For g, the data was mean \pm SD. Student's t -test was used for statistical analysis.

To further evaluate the broad applicability of OR@Lac to treat solid tumors, we tested its anticancer efficacy in 4T1 orthotopic model established using BALB/c female mice. Similar to the CT26 model, 4T1 tumor growth was significantly inhibited by administration of OR@Lac (Figure S4a–c, Supporting Information).

Furthermore, although the combination of OR and Lac delayed tumor growth, the antitumor effect was limited. In contrast, mice treated with the OR@Lac vaccine showed stronger tumor suppression, with 1/5 surviving to the end of the trial period and no tumor recurrence observed (Figure 5j,k). The above observation results unambiguously demonstrate the significant anti-cancer effects mediated by the immunomodulatory-modified *L. lactis* strategy, and our modified strategy was essential to maximize the synergistic effect of *L. lactis* and immune adjuvants.

2.5. In Vivo Immune Responses Triggered by OR@Lac

In our previous tumor inhibition experiments, the intratumoral administration of immunomodulators-modified *L. lactis* significantly inhibited tumor growth. As shown in Figure 6a, in order to evaluate the immune response elicited by OR@Lac, we replicated the tumor suppression experiment. Mice were euthanized and the tumor tissues and TDLNs were collected for immune response analysis one week after the last treatment. DCs and T cells play pivotal roles on the process of initiating and regulating both innate and adaptive immunities.^[32] Consequently, we initially explored whether this modification strategy could enhance DC maturation and facilitate effective infiltration of CTLs into tumor and TDLNs. Compared to control group, the percentage of mature DCs in the OR@Lac group (27.72%) exhibited a significant up-regulation, nearly tripling compared to the NS group (9.92%) (Figure 6b,c). TDLNs are crucial to activate naïve T cells by tumor antigen-loaded DCs. As demonstrated in Figure 6d, OR@Lac group induced a substantial increase of mature DCs in lymph nodes. The up-regulation of functional DCs indicated that DCs was in a more mature stage, in which CD8⁺ DCs increased by twofold compared to the NS group (Figure S5, Supporting Information). Correspondingly, the expression of CD3⁺CD8⁺T cells in the tumor and TDLNs of OR@Lac group was significantly higher than that of all treatment groups, indicating the elicitation of a strong cytotoxic T cell response within the tumor (Figure 6e–g). Consistent with the CT26 model, the analysis of immune microenvironment in the 4T1 tumor model showed a notable increase in the proportion of DCs and CD8⁺ T cells in both the tumor and lymph nodes (Figure S6a–h, Supporting Information).

Effector memory T cells (T_{EM}, CD3⁺CD8⁺CD44⁺CD62L[−]) have been demonstrated to induce potent immune protection. We observed a significant increase in the proportion of TEMs in the OR@Lac group (18.28%), while increased moderately without statistic difference in Lac group (13.93%) and OR group (13.78%) compared to untreated group (12.84%) (Figure 6h). Regarding macrophages, although there was no discernible difference in M1-like macrophages (CD11b⁺F4/80⁺CD86⁺) among all group (Figure S7, Supporting Information), a noteworthy decrease in the proportion of M2-like macrophages (CD11b⁺F4/80⁺CD206⁺) was observed, from 12.95% to 5.64%

(Figure 6i). Consistently, compared with control group, the proportion of M1and M2-like macrophages increased by ≈ 2.5 times (1.54 vs 3.88) (Figure 6j).

In addition, we extracted lymphocytes from the mice spleen in the NS and OR@Lac groups and co-cultured with CT26 tumor cells for 6 h. At 10:1 E: T in vitro, the OR@Lac group exhibited stronger cytotoxic activity, than NS group (Figure 6k; Figure S8, Supporting Information). These findings strongly indicate that the application of OR@Lac shaped a more immunogenic tumor microenvironment.

2.6. The Therapeutic Efficacy of the Combination of OR@Lac and Ibrutinib

Despite immune activation resulting in tumor regression after OR@Lac treatment, some tumors exhibited slow growth or recurrence (Figure 5d,e), indicating immune evasion of tumor cells. Through immunohistochemistry, we observed a significant presence of MDSCs within the tumor microenvironment of CT26 and 4T1 (Figure S9, Supporting Information). These MDSCs effectively suppressed the activity of immune cells, enabling tumor cells to evade attacks from the immune system, thus indicating that MDSC population can be an attractive therapeutic target. Ibrutinib has been shown to limit the production and migration of MDSCs, thereby improving the efficacy of cancer immunotherapies.^[20,33] Experiments have shown that ibrutinib reduced the expression of MDSC in tumor regardless of intraperitoneal or intratumoral injection (Figure 7a,b). We hypothesized that the inhibition of these MDSCs with ibrutinib could improve the clinical outcomes of IBL strategy. As illustrated in Figure 7c, OR@Lac-treated mice received ibrutinib three times. In combination with ibrutinib, OR@Lac further suppressed the growth of after the tumor inoculation (Figure 7d; Figure S10, Supporting Information). And the combination therapy of Ibrutinib + OR@Lac increased the percent survival from 40% in OR@Lac to 66.7% (4/6) (Figure 7e,f). Moreover, mice previously treated and cured with Ibrutinib+ OR@Lac were subjected to a rechallenge with CT26 tumors after 75 days. It is noteworthy that untreated mice exhibited rapid tumor growth, whereas mice treated with the combination of Ibrutinib+ OR@Lac showed a tumor suppression rate of 75% and survived for another 60 days (Figure 7g–i). In addition, the changes in body weight between the groups were almost negligible (Figure S11, Supporting Information). These results indicated the therapeutic potential of the combination of OR@Lac and MDSC inhibitor in clinical application.

3. Discussion

In this study, we have introduced an innovative approach utilizing IBL strategy to distribute therapeutic agents in solid tumors. As proof-of-concept research, we capitalized on the remarkable attributes of bacteria as effective drug vehicles to covalently modify Toll-like receptor agonists and immune checkpoint agonists onto the bacterial surface. Taking into consideration safety, practicality, and the careful selection of strains, we have chosen *L. lactis* as the ideal vehicle for drug delivery. The

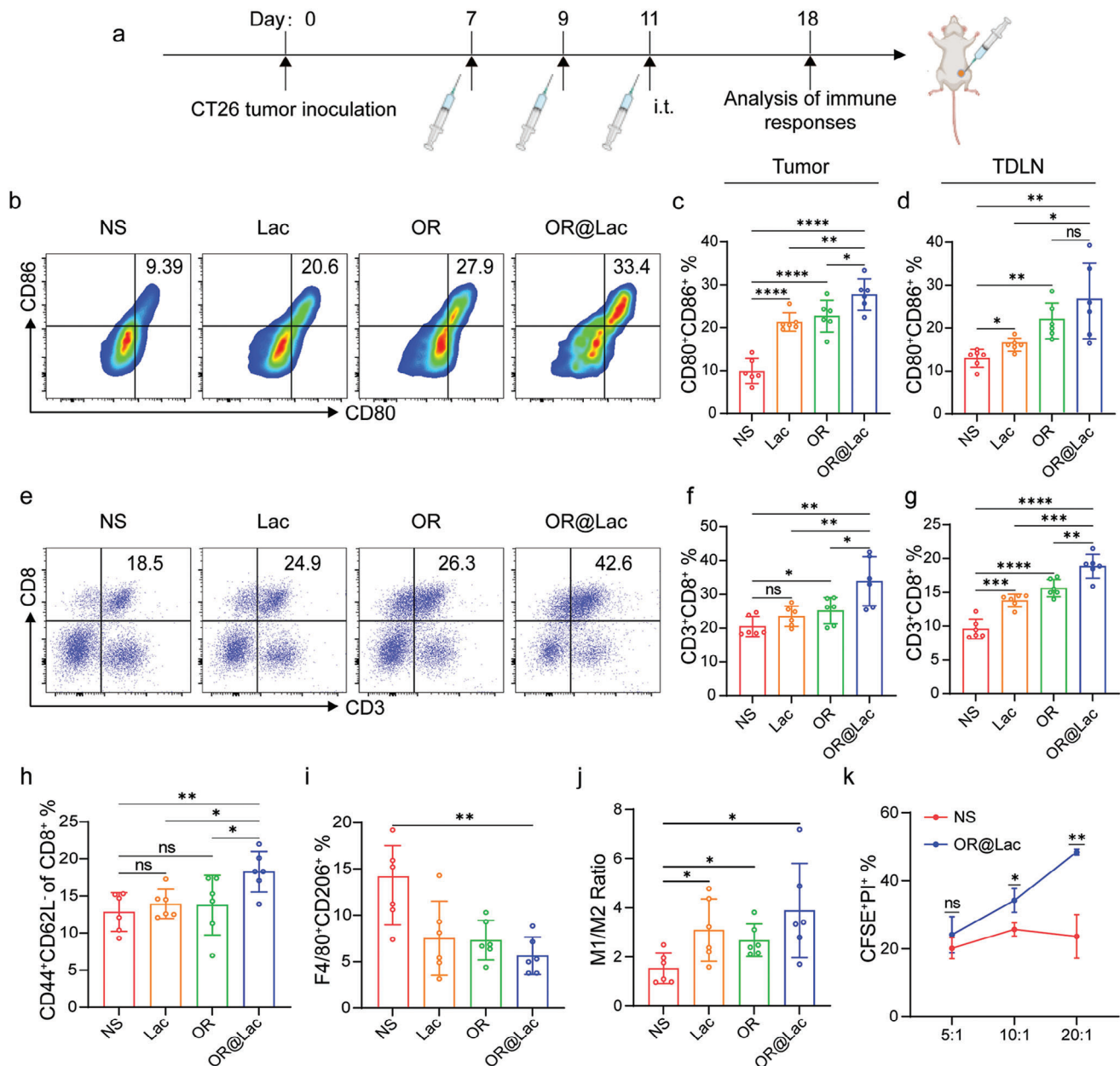


Figure 6. The strong intratumoral immune responses triggered by OR@Lac in CT26 tumor models. **a**) Scheme of treatment to analyze systemic immune responses. Representative flow cytometry images of CD80+CD86+ DCs (**b**), and CD3+CD8+ T cells (**e**) in the tumor microenvironment ($n = 6$). **c**, **d**) The percentage of CD80+CD86+ DCs in the tumor microenvironment and TDLN, respectively ($n = 6$). **f**, **g**) The percentage of CD3+CD8+ T cells in the tumor microenvironment and TDLN, respectively ($n = 6$). The flow cytometry analysis percentage of effector memory T cells (**h**), M2-like macrophages (**i**), and the ratio of M1/M2 (**j**) 7 days after treatments in the tumor microenvironment ($n = 6$). **k**) The percentage of dead cells was analyzed by flow cytometry under different target ratio ($n = 3$). For the experiments in (**c**, **d**), and (**f**–**k**), data was the mean \pm SD. Student's *t*-test was used for statistical analysis.

L. lactis-based IBL therapeutic strategy has several apparent advantages. 1) *L. lactis* itself has an adjuvant effect and can effectively activate DC cells. 2) Both proteins and small molecules can be modified onto the bacterial surface conveniently. 3) *L. lactis* are excellent carriers of molecules modified on them, which can increase the tumor retention time of these immune regulatory molecules and thus exert more sustained immune activation effects. 4) The mobile nature of bacteria may disperse immune reg-

ulatory molecules throughout the tumor tissues, which increases the chances of contact between immune regulatory molecules and immune cells within the tumor and improves the therapeutic effect of vaccines. In our study, α OX40 and R848 were attached to the surface of *L. lactis* to promote effective and long-lasting anti-tumor effect.

Immunosuppressive TME is a big obstacle that may limit the anti-tumor effect of cancer treatment, in which DCs and T cells

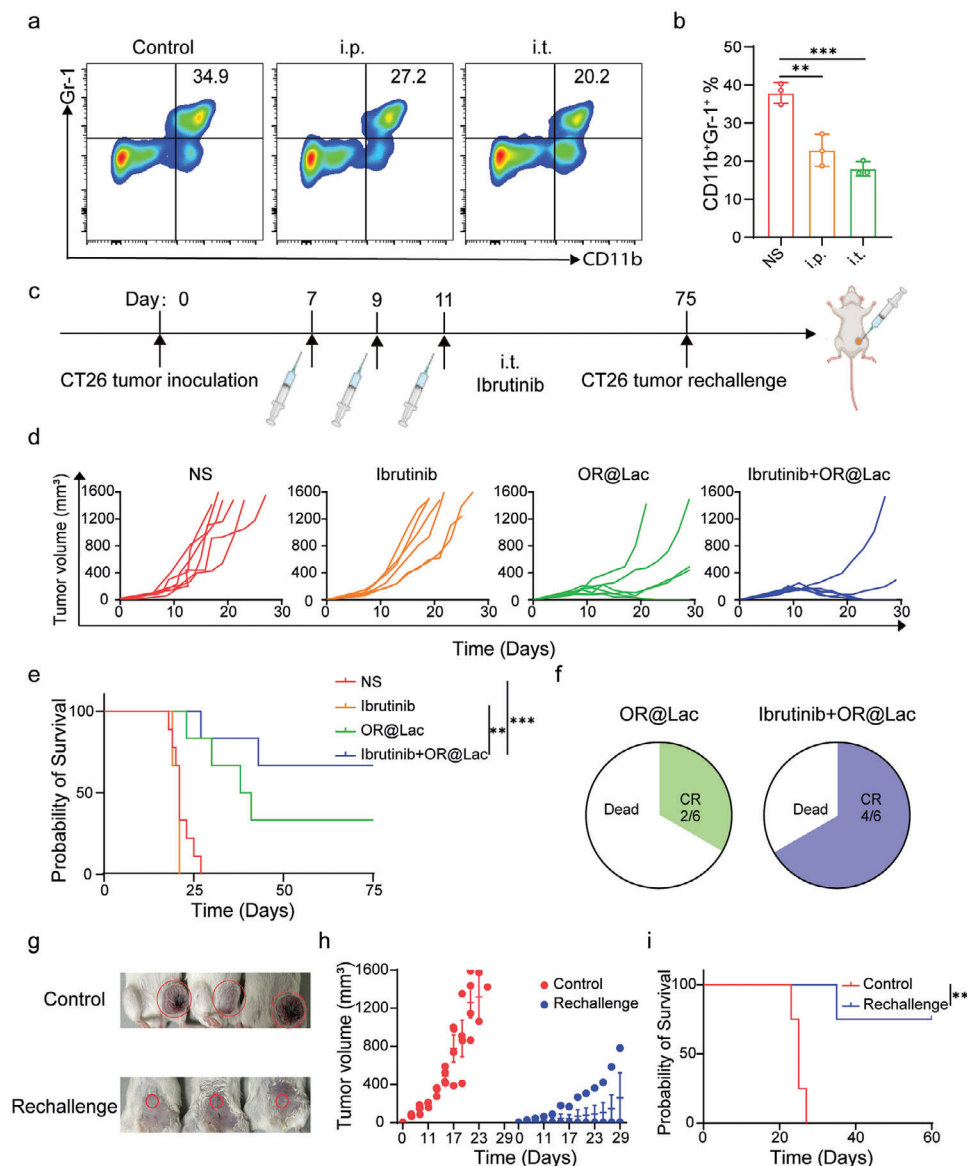


Figure 7. In vivo anti-tumor efficacy of OR@Lac combined with ibrutinib. a) Representative flow cytometry images of CD11b⁺Gr-1⁺ MDSC in the tumor microenvironment (n = 3). b) The percentage of CD11b⁺Gr-1⁺ MDSC in the tumor microenvironment (n = 3). c) Schematic diagram of the treatment in the tumor suppression experiment. d) The individualized tumor growth curves with (i) NS, (ii) ibrutinib (10 μg), (iii) OR@Lac (5 × 10⁸ CFU L. lactis contained 2 μg αOX40 and 5 μg R848), (iv) Simple mixture of ibrutinib and OR@Lac equal to (ii) and (iii), separately (n = 6). e) Survival data of CT26 mice treated with different treatments (n = 6). f) CR ratio pie chart. CR: complete response. g) The representative mice pictures were taken 20 days after the rechallenge (n = 3). Tumor growth curves (h), and Survival data (i) of each mouse following the rechallenge (n = 4). For the experiments in (e) and (h), the error bars show the mean ± SEM. *p*-values were calculated by two-way ANOVA with Tukey's multiple comparisons test and correction; survival differences were determined using Kaplan–Meier methods, and *p*-values were calculated using logarithmic rank (Mantel–Cox) tests.

play pivotal roles. We demonstrated that the IBL treatment strategy effectively activated DC in TME and TDLN, with a higher proportion of CD8⁺ DCs and CD80⁺CD86⁺ DCs, and further induce CD8⁺ T cells to exert anti-tumor effects, thus leading to systemic tumor regression. This strategy also showed a significant increase in the proportion of T_{EM} and decrease in the proportion of M2-like macrophages, indicating that OR@Lac successfully activated the innate and adaptive immune response, and formed long-term memory in CT26 tumor-bearing mice. Similar results were observed in 4T1 tumor-bearing mice, OR@Lac

greatly reversed the poor TME, triggered tumor-specific immune responses and systemic tumor regressions.

There are a large number of immunosuppressive suppressor cells in the TME, which have a negative impact on the immune system and thus promote tumor growth and escape. By immunohistochemical analysis, we found high expression of MDSCs in TME, which may be the reason for tumor relapse two weeks after the treatment in CT26 tumor-bearing mice or poor efficacy in 4T1 “cold” tumor models. Therefore, we combined immunomodulators modified L. lactis with an MDSC inhibitor to

induce a more powerful systemic immunotherapy effect for providing a more effective treatment strategy. Previous *in situ* vaccine studies predominantly centered around immune-activated molecules, our results successfully demonstrate that inhibiting immune-suppressive cells is also an effective method for enhancing vaccine efficacy.

While our study provides valuable insights, it is important to acknowledge its limitations. For instance, our focus on aminating drugs restricts the scope of bacterial modifications, and the generalizability of these findings to other probiotics remains unverified. Additionally, advancing single-cell transcriptomics is imperative to dissect gene-level variations and elucidate the immune cell regulatory dynamics within the TME. For future clinical translation, a comprehensive evaluation is warranted to address potential challenges. These include determining the optimal dosage of modified *L. lactis*, enhancing loading efficiency, and unraveling the mechanisms underlying immune cell modulation within the TME.

In summary, we described a strong rationale for using OR@Lac as an ISV. Given the simplicity and feasibility of this bacterial modification strategy, our study proposes a universal platform for IBL therapy in solid tumors, opening a new avenue for optimizing anti-tumor efficacy. This work also illustrates the promising application of highly tumor-specific immunotherapy enabled by the combined *L. lactis* and immunoadjuvants for comprehensive tumor therapeutics.

4. Experimental Section

Materials: N-(3-Dimethylaminopropyl)-N'-ethylcarbodiimide hydrochloride (EDC, >98%), N-hydroxysuccinimide (NHS, >98%) were purchased from Aladdin Reagent. Resiquimod (R848) and ibrutinib were obtained from MCE. Anti- α OX40 agonist antibody (α OX40, Clone OX-86) was purchased from Biorad. Monoclonal antibodies (mAbs) used in flow cytometry were listed as follows: PerCP/Cyanine5.5 anti-mouse CD3, PerCP/Cyanine7 anti-mouse CD4, FITC anti-mouse CD8, PE anti-mouse CD44, APC anti-mouse CD62L, APC anti-mouse CD25, APC anti-mouse CD69, PE anti-mouse CD11c, APC anti-mouse CD80, PerCP/Cyanine7 anti-mouse CD86, PerCP/Cyanine5.5 anti-mouse CD11b, APC anti-mouse F4/80, PE anti-mouse CD206, PE anti-mouse FOXP3, FITC anti-mouse Gr-1. All antibodies were purchased from Biolegend and diluted in 1:100. Cytokines were detected with the Biolegend 8-factor kit.

Mice: The 6–7 weeks male/female BALB/c mice were purchased from GemPharmatech (Nanjing, China) and raised in specific pathogen-free (SPF) Laboratory of the Animal Center of Affiliated Nanjing Drum Tower Hospital of Nanjing University Medical School (Nanjing, China). All procedures were carried out in accordance with the guidelines approved by the Animal Ethics Committee of Nanjing Drum Tower Hospital (Grant No. 2023AE01052).

Cell Lines: CT26 and 4T1 were kept in the Oncology Laboratory, they were cultured in RPMI 1640 complete medium supplemented containing 10% fetal bovine serum, 100 U mL⁻¹ penicillin, and 100 μ g mL⁻¹ streptomycin.

Preparation of OR@Lac: Amino-functionalized R848 and OX40 agonists were linked on the surface of *L. lactis* by amide condensation. In short, 5×10^9 CFU *L. lactis* NZ9000 were collected and dispersed at 500 μ l PBS (Corning, New York, USA) through 4500 rpm, centrifuged for 10 min., and then 100 μ l of amino-functionalized R848 (1 mg mL⁻¹), 3.1 mg EDC and 3.45 mg NHS were added into the bacterial suspension and rotated 2 h at room temperature. The role of EDC and NHS is described in the literature in the amide condensation process.^[34] After 2 h, R@Lac was obtained by centrifugation at 4500 rpm for 10 min and washed with PBS for three times. Second, disperse R@Lac at 500 μ l PBS solution, and 50 μ l

amino functionalization α OX40 (1 mg mL⁻¹), 3.1 mg EDC, and 3.45 mg NHS were added to the *L. lactis* suspension together. After rotating for 2 h, the above operations were repeated to obtain double-drug modified *L. lactis*.

Characterization of OR@Lac: The size distribution and zeta potential of *L. lactis*, OR@Lac were measured by dynamic light scattering (DLS) on a Zetasizer Nano ZS90 (Malvern, UK). To confirm the α OX40 was incorporated onto bacterial surface, cy5.5-conjugated α OX40 was employed and measured by using flow cytometry (Beckman CytoFLEX, USA). The loading efficiencies of α OX40 and R848 were separately measured using high-performance liquid chromatography (HPLC). The detection wavelengths were 280 and 254 nm and the HPLC test template was set (flow rate, 1 mL min⁻¹; mobile phase comparison, (A) acetonitrile containing 1% TFA and (B) water containing 1% TFA; α OX40, the concentration of A in the mobile phase ranged from 5% to 65%, 15 min; R848, the concentration of A in the mobile phase ranged from 5% to 65%, 10 min) and determined at different concentrations (1000, 500250125, 62.5, 31.25, and 15.625 μ g mL⁻¹), after which the standard curve was plotted. The loading efficiency were derived from the following Equation (1):

$$\text{Loading Efficiency (\%)} = 1 - \frac{\text{weight of the drug in supernatant}}{\text{weight of the feeding drug}} \times 100\% \quad (1)$$

Growth Curves of Conjugated *L. lactis*: Equal amounts of uncoated *L. lactis*, R848, and α OX40 coated probiotic (OR@Lac) were diluted in GM17 medium to reach the same initial optical density at 600 nm (OD600) and incubated at 30°. The OD values of cultures were recorded at 600 nm every 2 h for 12 h by UV/Vis.

In Vitro BMDCs Uptake of *L. lactis*: Bone marrow-derived dendritic cells (BMDCs) were isolated from bone marrow mesenchymal stem cells of 6–7 weeks BALB/c mouse. Then the cells were cultured in RPMI 1640 complete medium containing 20 ng mL⁻¹ mGM-CSF (Xiamen Amoytop Biotech Co., Ltd., China) and 10 ng mL⁻¹ rIL-4 (Pepro Tech, USA), followed by specific operations as described in the previous literature.^[16]

Maturation and Activation of BMDCs: After 8 days of BMDCs cultivation, immature BMDCs (2 \times 10⁵ cells/well) were seeded in 96-well plates and severally treated with NS, *L. lactis* (1 \times 10⁷ mL⁻¹), R848+ α OX40 (OR, 1 μ g mL separately), OR @Lac (1 μ g R848 and α OX40 were loaded at 1 \times 10⁷ CFU mL⁻¹ on *L. lactis*), and lipopolysaccharide (LPS, 1 μ g mL⁻¹) for 24 h. Afterward, DCs were collected and suspended in PBS, and then cells were incubated with anti-mouse antibodies (CD11c, CD80, and CD86) for 30 min at 4° in the dark. Subsequently, data were obtained by Flow cytometry and analyzed using Flowjo software. The proinflammatory cytokines (i.e., IL-6, TNF- α , and IFN- γ) in suspension were detected by LEGENDplex MU Th1/Th2 Panel (8-plex) w/VbP V03 (Biolegend, USA) with a standard protocol and analyzed using Biolegend online data analysis software.

In Vitro T-Cell Activation: First, T cells were collected from the spleen of 8–10 weeks BALB/c mice, after which they were cultured in AIMV medium containing 10% FBS, 1% penicillin-streptomycin, 24 IU mL⁻¹ IL-2 and 50 ng mL⁻¹ IL-7. Second, immature BMDCs were cultured in 96-well plates and treated with NS, Lac, OR, OR@Lac for 24 h at 37°. Subsequently, the drug-treated DCs were co-cultured with T cells at a ratio of 1:5. After 72 h, the cells were collected by centrifugation and assessed by flow cytometry analysis of the expression of CD4⁺CD69⁺ and CD8⁺CD69⁺.

In Vivo Real-Time Near-Infrared Fluorescence Imaging: *L. lactis* were quantitatively located by near-infrared imaging. Intratumoral injection of *L. lactis* labeled with DiR (Bridgen, Beijing, China). We anesthetized and scanned mice at designated time points (6, 24, 72, 168, and 360 h) using the CRi Maestro In Vivo Imaging System (Cambridge Research & Instrumentation, Massachusetts, USA). Subsequently, tumors, TDLNs, and vital organs of the mice were excised and imaged, and fluorescence measurements were analyzed using Living Imaging software.

Intratumoral Distribution of cy5.5-IgG@Lac: Cyanine 5.5 (cy5.5)-conjugated IgG was employed to replace α OX40. The cy5.5-IgG@Lac was prepared according to the method described for α OX40@Lac. Subcutaneous CT26 tumor-bearing mice were intratumorally injected with 100 μ l

cy5.5-IgG@Lac or free cy5.5-conjugated IgG at a dose of 20 µg IgG per mouse. At 72 h after injection, tumors, TDLNs, and central organs of the mice, were dissected, and the fluorescence detection was analyzed using Living Imaging software.

Animal Experiments: Two cell lines, CT26 and 4T1, were used to observe the antitumor effect in vivo. The cells were suspended at a dose of 2.0×10^6 per mouse in 100 µl PBS into the left flanks of male or female BALB/c mice (6 weeks old). The tumors were randomly divided into four groups once they reached 80–100 mm³, tumor were treated intratumorally with NS, 5×10^8 CFU *L. lactis*, 5 µg R848+2 µg αOX40, and 5×10^8 CFU OR@Lac loaded with 5 µg R848 and 2 µg αOX40 on days 7, 9, and 11. Subsequently, tumor volume was detected every other day, and calculated it by the formula length \times width²/2. When the tumor volume reached 1500 mm³ or the maximum tumor diameter reached 20 mm, the mice were euthanized immediately. In order to observe the response of immune cells, mice were euthanized one week after the last administration, tumors and lymph nodes were collected and single cell suspension was prepared for flow cytometry. At the same time, the central organs were taken, fixed with 4% paraformaldehyde and embedded in paraffin, stained with hematoxylin and eosin (H&E), and analyzed under a light microscope (Leica DM5000, Germany) for safety.

Flow Cytometry: The tumor tissues, TDLNs, and spleens were taken out from the mice, and then using mechanical trituration the spleens and TDLNs were made into single-cell suspension. At the same time, the tumor tissues were cut into small pieces and digested with collagenase type IV (1 mg ml⁻¹, Sigma) for 2 h at 37 ° with gentle agitation. Then all cell samples were resuspended in pre-cooled PBS and stained with specific antibodies for 30 min at 4 ° in darks, and then washed before analysis.

Cytotoxicity Assay of Mouse Splenocytes: CT26 colon cancer cells were stained with CFSE at 37 ° for 10 min in darks. Spleen cells in NS group and OR@Lac group were incubated with CFSE-labeled CT26 cells at an effective target ratio of 5:1, 10:1, and 20:1, respectively. After 6 h, the mixed cells were stained with PI for 10 min at 4 ° in darks, and then washed and analyzed on Flow cytometry.

Statistical Analysis: Statistical analysis and graphs were conducted by Graphpad Prism 8.0 (SanDiego, CA). Figures were designed in Adobe Illustrator 2021. All experiments were repeated at least three times. The unpaired student's *t*-test was used for pair-wise comparisons, the one-way ANOVA with Tukey's multiple comparisons was selected for multiple comparisons and the Kaplan-Meier method was employed for survival analysis. The results were expressed as mean \pm SD or mean \pm SEM. **p* < 0.05, ***p* < 0.01, ****p* < 0.001, *****p* < 0.0001 were considered statistically significant.

Supporting Information

Supporting Information is available from the Wiley Online Library or from the author.

Acknowledgements

M.S. and T.S. contributed equally to this work. This work was supported by the National Natural Science Foundation of China (Grant No. 82373280 and 82072926). F.M., B.L., and R.L. designed the study. M.S. and T.S. conducted experiments and interpreted the results. S.T., M.L., Q.W., C.L., L.Z., Q.Z., Y.W., and J.D. assisted with the experimental work. M.S. and T.S. prepared the manuscript. F.M., R. L., and B.L. supervised the research and verified the results. All authors critically reviewed and approved the final version of the manuscript.

Conflict of Interest

The authors declare no conflict of interest.

Data Availability Statement

The data that support the findings of this study are available from the corresponding author upon reasonable request.

Keywords

drug delivery, lactococcus lactis, tumor immunotherapy, tumor microenvironment, tumor vaccines

Received: May 3, 2024

Revised: July 15, 2024

Published online:

- [1] W. X. Hong, I. Sagiv-Barfi, D. K. Czerwinski, A. Sallets, R. Levy, *Cancer Res.* **2022**, *82*, 1396.
- [2] A. Marabelle, L. Tselikas, T. De Baere, R. Houot, *Ann. Oncol.* **2017**, *28*, xii33.
- [3] I. Sagiv-Barfi, D. K. Czerwinski, S. Levy, I. S. Alam, A. T. Mayer, S. S. Gambhir, R. Levy, *Sci. Transl. Med.* **2018**, *10*, aar4488.
- [4] Z. Sun, Y. Chu, J. Xiao, Y. Yang, F. Meng, X. Wang, Y. Dong, J. Zhu, Y. Wu, L. Qin, Y. Ke, B. Liu, Q. Liu, *J. Transl. Med.* **2023**, *21*, 619.
- [5] K. Sugamura, N. Ishii, A. D. Weinberg, *Nat. Rev. Immunol.* **2004**, *4*, 420.
- [6] J. Willoughby, J. Griffiths, I. Tews, M. S. Cragg, *Mol. Immunol.* **2017**, *83*, 13.
- [7] T. W. Kim, H. A. Burris, M. J. de Miguel Luken, M. J. Pishvaian, Y.-J. Bang, M. Gordon, A. Awada, D. R. Camidge, F. S. Hodi, G. A. McArthur, W. H. Miller, A. Cervantes, L. Q. Chow, A. M. Lesokhin, A. Rutten, M. Sznol, D. Rishipathak, S.-C. Chen, E. Stefanich, T. Pourmohamad, M. Anderson, J. Kim, M. Huseni, I. Rhee, L. L. Siu, *Clin. Cancer Res.* **2022**, *28*, 3452.
- [8] E. J. Davis, J. Martin-Liberal, R. Kristeleit, D. C. Cho, S. P. Blagden, D. Berthold, D. B. Cardin, M. Vieito, R. E. Miller, P. Hari Dass, A. Orcurto, K. Spencer, J. E. Janik, J. Clark, T. Condamine, J. Pulini, X. Chen, J. M. Mehnert, *J. Immunother. Cancer* **2022**, *10*, e004235.
- [9] Y. Chu, R. Li, L. Qian, F. Liu, R. Xu, F. Meng, Y. Ke, J. Shao, L. Yu, Q. Liu, B. Liu, *Cancer Sci.* **2021**, *112*, 4490.
- [10] G. Ji, Y. Zhang, X. Si, H. Yao, S. Ma, Y. Xu, J. Zhao, C. Ma, C. He, Z. Tang, X. Fang, W. Song, X. Chen, *Adv. Mater.* **2021**, *33*, 2004559.
- [11] K. G. Nguyen, M. R. Vrabell, S. M. Mantooth, J. J. Hopkins, E. S. Wagner, T. A. Gabaldon, D. A. Zaharoff, *Front. Immunol.* **2020**, *11*, 575597.
- [12] X. Shen, C. Zhu, X. Liu, H. Zheng, Q. Wu, J. Xie, H. Huang, Z. Liao, J. Shi, K. Nan, J. Wang, X. Mao, Z. Gu, H. Li, *Biomater. Sci.* **2023**, *11*, 1137.
- [13] C.-N. Ko, S. Zang, Y. Zhou, Z. Zhong, C. Yang, *J. Nanobiotechnol.* **2022**, *20*, 380.
- [14] S. Singha, K. Shao, K. K. Ellestad, Y. Yang, P. Santamaria, *ACS Nano* **2018**, *12*, 10621.
- [15] S. Wilhelm, A. J. Tavares, Q. Dai, S. Ohta, J. Audet, H. F. Dvorak, W. C. W. Chan, *Nat. Rev. Mater.* **2016**, *1*, 16014.
- [16] J. Zhu, Y. Ke, Q. Liu, J. Yang, F. Liu, R. Xu, H. Zhou, A. Chen, J. Xiao, F. Meng, L. Yu, R. Li, J. Wei, B. Liu, *Nat. Commun.* **2022**, *13*, 7466.
- [17] R. Garza-Morales, B. E. Rendon, M. T. Malik, J. E. Garza-Cabral, A. Aucouturier, L. G. Bermúdez-Humarán, K. M. McMasters, L. R. McNally, J. G. Gomez-Gutierrez, *Cancers* **2020**, *12*, 438.
- [18] A. Michaelis, M. A. Norgard, X. Zhu, P. R. Levesseur, S. Sivagnanam, S. M. Liudahl, K. G. Burfeind, B. Olson, K. R. Pelz, D. M. Angeles Ramos, H. C. Maurer, K. P. Olive, L. M. Coussens, T. K. Morgan, D. L. Marks, *Nat. Commun.* **2019**, *10*, 4682.
- [19] B. Bahmani, H. Gong, B. T. Luk, K. J. Haushalter, E. DeTeresa, M. Previti, J. Zhou, W. Gao, J. D. Bui, L. Zhang, R. H. Fang, J. Zhang, *Nat. Commun.* **2021**, *12*, 1999.
- [20] A. Stiff, P. Trikha, R. Wesolowski, K. Kendra, V. Hsu, S. Uppati, E. McMichael, M. Duggan, A. Campbell, K. Keller, I. Landi, Y. Zhong, J. Dubovsky, J. H. Howard, L. Yu, B. Harrington, M. Old, S. Reiff,

- T. Mace, S. Tridandapani, N. Muthusamy, M. A. Caligiuri, J. C. Byrd, W. E. Carson, *Cancer Res.* **2016**, 76, 2125.
- [21] G. D. Shockman, J. F. Barrett, *Annu. Rev. Microbiol.* **1983**, 37, 501.
- [22] J.-X. Fan, M.-Y. Peng, H. Wang, H.-R. Zheng, Z.-L. Liu, C.-X. Li, X.-N. Wang, X.-H. Liu, S.-X. Cheng, X.-Z. Zhang, *Adv. Mater.* **2019**, 31, 1808278.
- [23] D. Pum, M. Sara, U. B. Sleytr, *J. Bacteriol.* **1989**, 171, 5296.
- [24] S. Hovmoller, A. Sjogren, D. N. Wang, *Prog. Biophys. Mol. Biol.* **1988**, 51, 131.
- [25] B. J. Toley, N. S. Forbes, *Integr. Biol.* **2012**, 4, 165.
- [26] J. E. Boudreau, A. Bonehill, K. Thielemans, Y. Wan, *Mol. Ther.* **2011**, 19, 841.
- [27] J. Banchereau, F. Briere, C. Caux, J. Davoust, S. Lebecque, Y.-J. Liu, B. Pulendran, K. Palucka, *Annu. Rev. Immunol.* **2000**, 18, 767.
- [28] J. P. Vasilakos, M. A. Tomai, *Expert Rev. Vaccines* **2013**, 12, 809.
- [29] F. Wang, H. Su, D. Xu, W. Dai, W. Zhang, Z. Wang, C. F. Anderson, M. Zheng, R. Oh, F. Wan, H. Cui, *Nat. Biomed. Eng.* **2020**, 4, 1090.
- [30] Z. Xiao, C. Ji, J. Shi, E. M. Pridgen, J. Frieder, J. Wu, O. C. Farokhzad, *Angew. Chem. Int. Ed. Engl.* **2012**, 51, 11853.
- [31] A. Huang, M. M. Pressnall, R. Lu, S. G. Huayamates, J. D. Griffin, C. Groer, B. J. DeKosky, M. L. Forrest, C. J. Berkland, *J. Control Release* **2020**, 326, 203.
- [32] L. Huang, Y. Li, Y. Du, Y. Zhang, X. Wang, Y. Ding, X. Yang, F. Meng, J. Tu, L. Luo, C. Sun, *Nat. Commun.* **2019**, 10, 4871.
- [33] I. Sagiv-Barfi, H. E. K. Kohrt, D. K. Czerwinski, P. P. Ng, B. Y. Chang, R. Levy, *Proc. Natl. Acad. Sci. USA* **2015**, 112, E966.
- [34] Z. Geng, Z. Cao, R. Liu, K. Liu, J. Liu, W. Tan, *Nat. Commun.* **2021**, 12, 6584.